Alexandria Engineering Journal (2016) 55, 2257–2268

HOSTED BY

Alexandria University

Alexandria Engineering Journal

www.elsevier.com/locate/aej
www.sciencedirect.com

ORIGINAL ARTICLE

Numerical investigation of distance effect between two Searasers for hydrodynamic performance

Ali A. Babajani [a,*], Mohammad Jafari [b], Parinaz Hafezi Sefat [c]

[a] Department of Mechanical Engineering, Shahrekord University, Shahrekord 53849-88176, Iran
[b] Department of Mechanical Engineering, Sharif University of Technology, Tehran 11365-9567, Iran
[c] Department of Chemical Engineering, Isfahan University of Technology, Isfahan 84156-83111, Iran

Received 28 January 2016; revised 18 April 2016; accepted 18 May 2016
Available online 11 June 2016

KEYWORDS

Searaser;
Wave energy;
Numerical simulation;
Wave energy convertor

Abstract Nowadays, researchers are interested in investigation of the ocean wave energy conversion (OWEC) because this device can convert wave energy into electricity economically. The aim of this study was to evaluate a novel ocean wave energy converter named Searaser which may be capable of being used in the Caspian Sea. One of the ways for improving the efficiency of Searasers is to use numerous Searasers simultaneously. Increasing the number of Searasers not only increases the electricity production but also can help producing more stable electricity. In this article the function of two Searasers three different distances (10, 15 and 20 m) was evaluated numerically by solving momentum and continuity equations in unsteady condition by FLOW-3D software. The effect of different wave heights of Caspian Sea was also investigated in this research. To evaluate the numerical results of this research, they were also compared with experimental results of modeling a buoy and showed good agreement. For the three mentioned distances of buoys, the outlet flow rate and the buoys movement were measured. The results showed that when the buoys were 15 m far from each other, the hydrodynamic performance was better and the outlet flow rate and electricity generation showed less fluctuation.

1. Introduction

Ocean wave energy has great potential in supplying worldwide demand for power. After oil crisis in 1970s, wave energy attracts more attention but few people have heard of ocean wave energy capabilities. Actually hydroelectric dams are the best known water-based energy sources, but wave energies are good replacement to supply increasing demand for electricity [1]. Nowadays widespread concern of global climate change, environmental hazards and rising prices of fossil fuels has attracted more interest in renewable energies such as wave energy.

Wave energy devices can be categorized by energy conversion principle in four different groups of oscillating water column, overtopping device, attenuator, and point absorber. In oscillating water column (OWC) air compression and decompression cause the water to go upward and downward the column and as a result the water drives turbine. The spare buoy is the simple form of OWCs. The OWC spar-buoy is basically

* Corresponding author.
E-mail address: a.babajani@stu.sku.ac.ir (A.A. Babajani).
Peer review under responsibility of Faculty of Engineering, Alexandria University.

http://dx.doi.org/10.1016/j.aej.2016.05.022

consisted of long submerged vertical tail tube that is open at both ends and moves with waves. The OWC spar buoy with a tube of uniform cross section was the object of the first publications of OWCs.

In the second group, an overtopping WEC captures seawater in a reservoir that is located above the sea level and then releases the water back to the sea via a number of low-head turbines connected to a generator. Some familiar examples of overtopping devices are Wave Dragon [2], SSG [3–5] and WaveCat [6].

In the third group, the attenuators have multiple floating segments that are connected to each other and also these buoys are parallel to the wave direction. These segments move in relation to each other with incoming waves. This relative motion pumps high pressure oil through hydraulic motors and generates electricity. Pelamis is an offshore, floating, snake-like device consisting of semi-submerged cylinders connected to each other [7,8]. As the other types, there are famous attenuators such as Wave Star [9], Salter Duck [10] and Anaconda [11].

In the last group, the buoy type wave energy converter is known as point absorber because it absorbs energy from all directions at one point. The buoys use the vertical motion of waves for compressing gas or liquid; then this fluid drives the power generator and can produce electricity. Most of the times point absorbers are placed far from shoreline in different ocean depths from shallow to very deep waters [12]. Point absorbers have great potential to generate electricity from small devices [13].

In 2013, Alvin Smith [14] invented a novel OWEC named Searaser based on the registered patent. According to the inventor's patent, this invention has exceptional benefits rather than other types of OWECs, which will be mentioned in Section 2 (Description of Searaser) completely. In the present study, attempts have been made to simulate the Searaser performance in the wave tank by solving Navier–Stokes equations. Therefore, a commercial CFD code (Flow-3D) which is suitable for modeling of WEC has been used to solve the governing equations. In order to validate the hydrodynamic results, firstly the hydrodynamic performance of a point absorber was investigated via this software in which the difference of numerical and experimental data was negligible. In this article two Searasers were simulated numerically in different distances to find an optimum distance between these two devices where they can produce more electrical energy.

2. Description of Searaser

Searaser is a novel technology that was invented by Alvin Smith and registered as a patent in 2013 [14]. It can be used as a water pump for generating power. The Searaser is shown schematically in Fig. 1a. As it can be seen the Searaser consists of a cylinder attached to a piston, in which the piston moves upward by buoyancy force when the waves reach the vicinity of Searaser and it moves downward with the gravity when the wave passes. The cycle of generating electricity is shown in Fig. 1b. As it is clear in this figure, Searasers pump water to a higher level reservoir in onshore zone by rolling motion of the waves, and then accumulated water returns to the sea after passing the turbines and generating electricity.

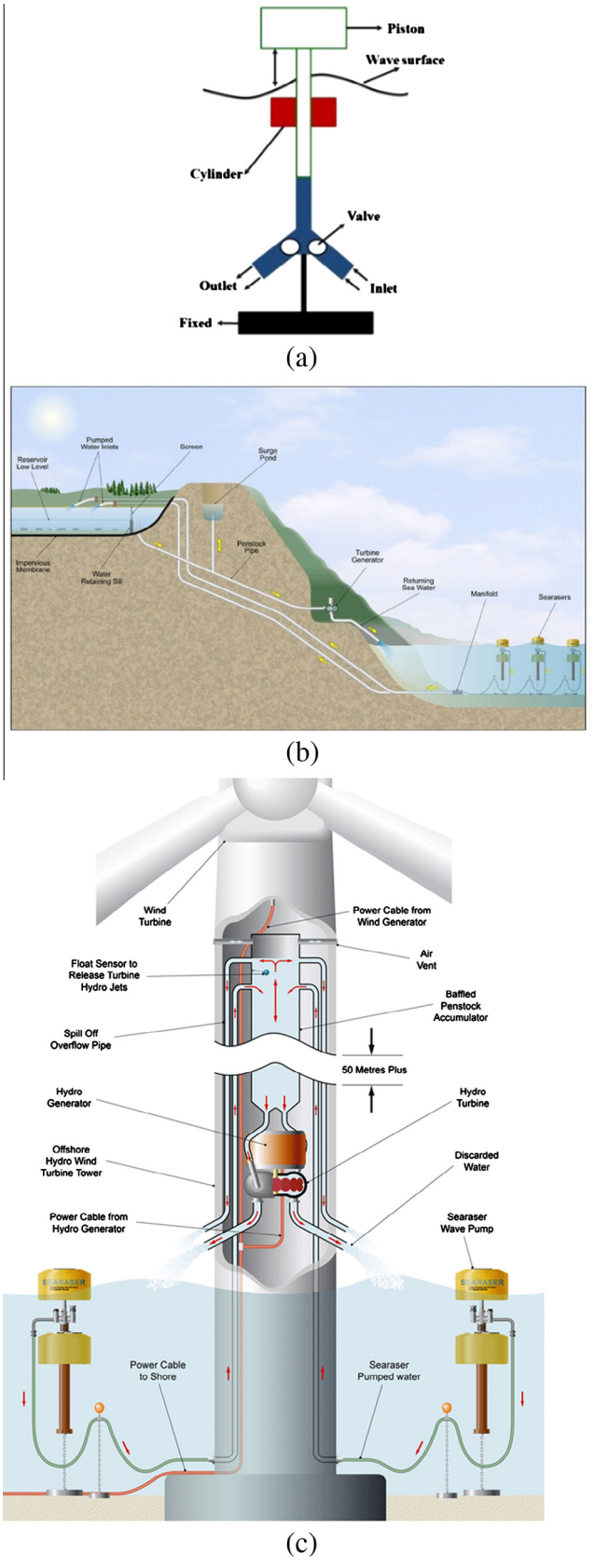

Figure 1 (a) Different components of Searaser, (b) cycle of electricity generation via Searaser, (c) transferring output water from Searaser inside wind turbine.

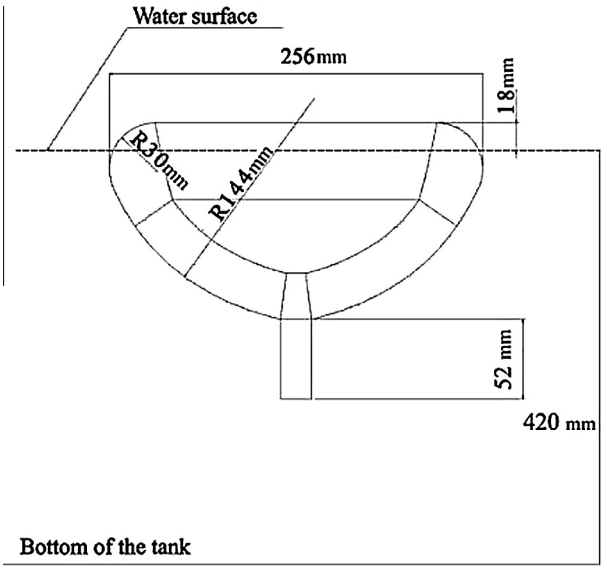

Figure 2 Geometry and dimensions of simulated point absorber (WRASPA).

Searaser is a simple device with cheaper components in comparison with other types of WECs because the components

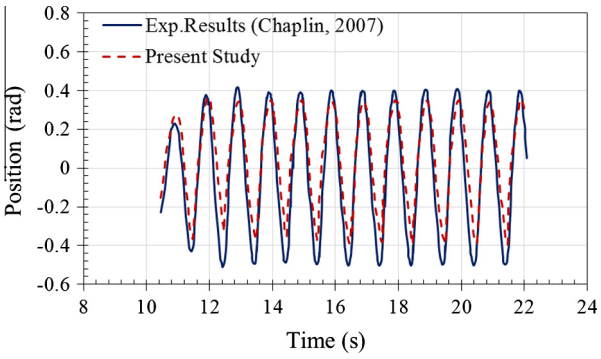

Figure 4 Comparison of numerical and experimental results for angular rotation.

that produce electricity (turbine and generator) are separated from Searaser and it is also really beneficial because generating electricity in offshore area is so hard due to corrosion problems. Another important benefit of Searasers is that during the process of producing electricity there is no gas emission so it is completely green. As it is shown in Fig. 1c the output water of the Searasers can be transferred to the place where

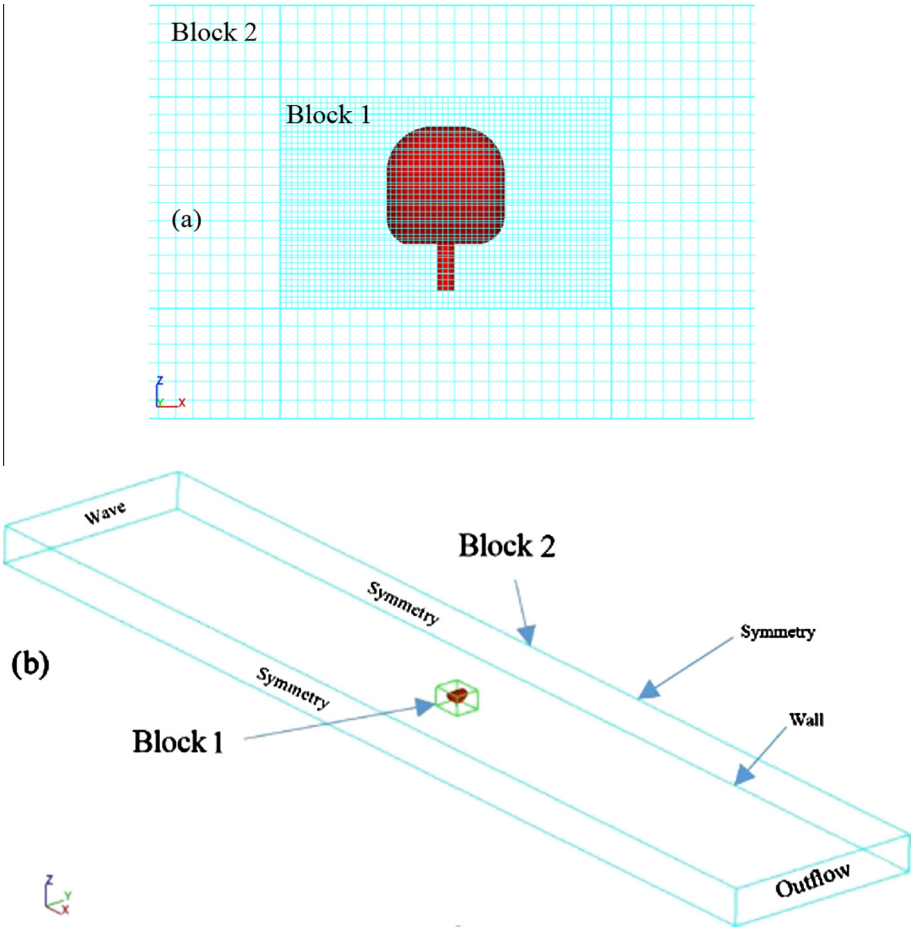

Figure 3 (a) Schematic of meshing the wave tank and WRASPA, (b) axis and dimensions including boundary conditions.

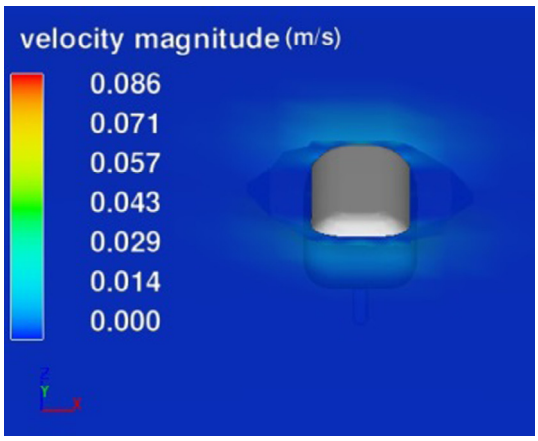

(a) t=1.09s

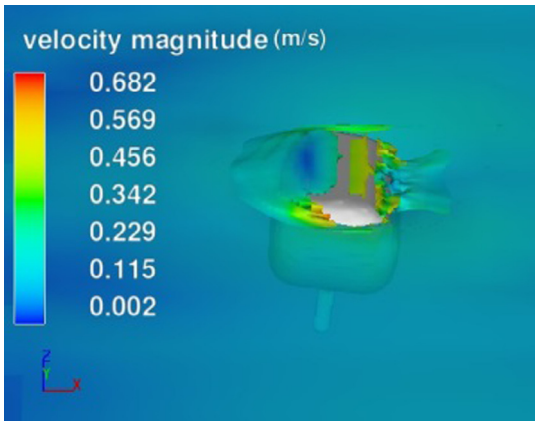

(b) t=15.75s

Figure 5 Velocity contour for simulated WRASPA: (a) $t = 1.09$ s, (b) $t = 15.75$ s.

wind turbines are located, and as a result the efficiency will be improved.

3. Governing equations

3.1. Equations of movement (rigid body)

In general, each motion of a rigid body can be divided into translational and rotational movements. The velocity of each single moving point is equal to the optional base point velocity plus the velocity that is originated from the rotation of the body around the base point. For movement in 6 degrees of freedom, the general moving object (GMO) model considers the mass center of the body (G) as the base point. The equations for 6 degree of freedom movement are divided into two separate following equations [13]:

$$\overrightarrow{F} = m\frac{d\overrightarrow{V_G}}{dt} \tag{1}$$

$$\overrightarrow{T_G} = [J]\cdot\frac{d\vec{\omega}}{dt} + \vec{\omega}\times([J]\cdot\vec{\omega}) \tag{2}$$

$\vec{\omega}$ is the angular velocity (rad/s), $\overrightarrow{V_G}$ is the velocity of mass center (m/s), $\vec{F}$ is the total force (N), m is the mass of the rigid body (kg), $\overrightarrow{T_G}$ is the total torque (N m) about G and $[J]$ is the moment of inertia tensor (kg m^2) about G in a body proportional referenced system. The total force and total torque are calculated as the summation of some different components as follows:

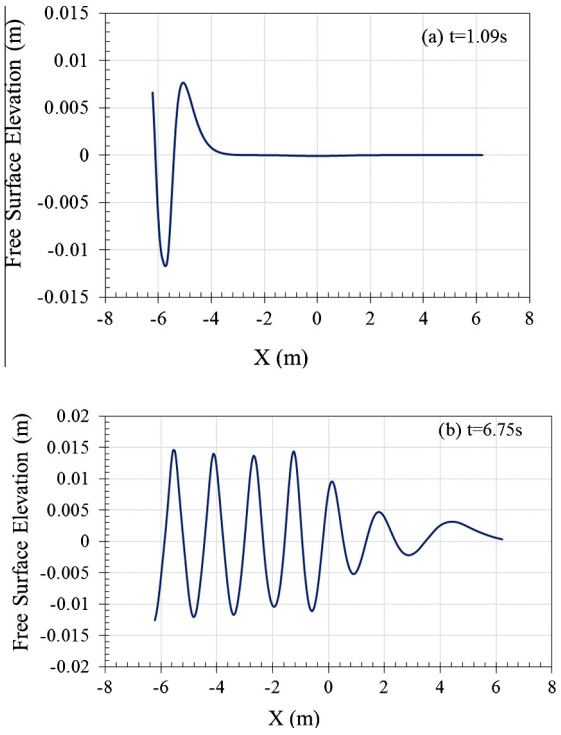

Figure 6 Free surface elevation of wave for different times: (a) $t = 1.09$ s, (b) $t = 6.75$ s.

$$\overrightarrow{F} = \overrightarrow{F_g} + \overrightarrow{F_h} + \overrightarrow{F_c} + \overrightarrow{F_{ni}} + \overrightarrow{F_i} \tag{3}$$

$$\overrightarrow{T_G} = \overrightarrow{T_g} + \overrightarrow{T_h} + \overrightarrow{T_c} + \overrightarrow{T_{ni}} \tag{4}$$

where $\overrightarrow{F_g}$ is the gravitational force, $\overrightarrow{F_h}$ is the hydraulic force that is due to pressure field and shear forces of the wall on the moving body, $\overrightarrow{F_c}$ is the net control force of the network that can be used for controlling and confining the rigid body motion. $\overrightarrow{F_{ni}}$ is the non-inertial force when the rigid body moves in a non-inertial space system, so in this case there are no $\overrightarrow{F_{ni}}$, $\overrightarrow{T_G}$, $\overrightarrow{T_g}$, $\overrightarrow{T_h}$, $\overrightarrow{T_c}$, and $\overrightarrow{T_{ni}}$ which are the total torque, gravitational torque, hydraulic torque, control torque and non-inertial torque around the mass center of the rigid body respectively. The continuity and momentum equations for a moving body and the relative transport equations for the volume of the fluid function (VOF) are as follows:

$$\frac{V_f}{\rho}\frac{\partial\rho}{\partial t} + \frac{1}{\rho}\nabla.(\rho\vec{u}A) = -\frac{\partial V_f}{\partial t} \tag{5}$$

$$\frac{\partial\vec{u}}{\partial t} + \frac{1}{V_f}(\vec{u}A_f.\nabla\vec{u}) = -\frac{1}{\rho}\left[\nabla p + \nabla.(\tau A_f)\right] + \overrightarrow{G} \tag{6}$$

$$\frac{\partial F}{\partial t} + \frac{1}{V_f}\nabla.(F\vec{u}A_f) = -\frac{F}{V_f}\frac{\partial V_f}{\partial t} \tag{7}$$

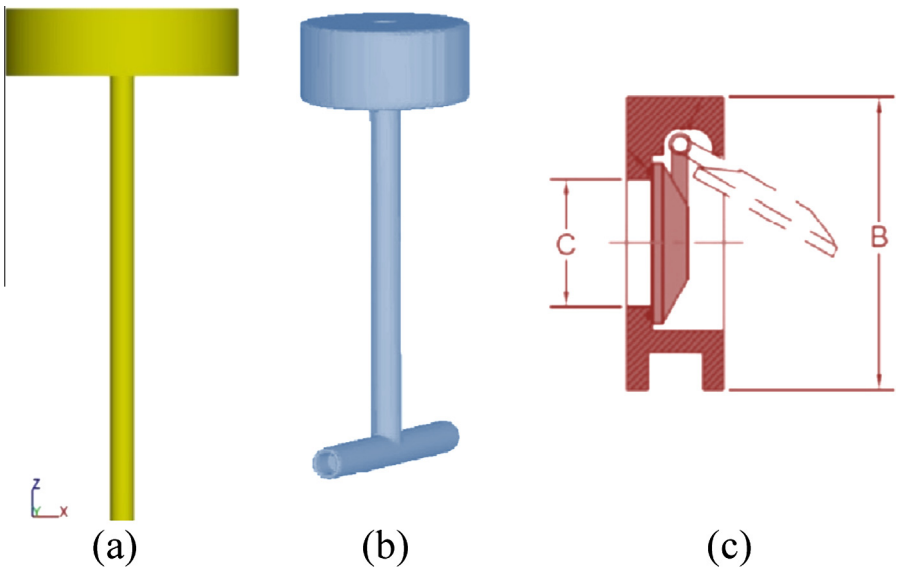

Figure 7 (a) Schematic of first component-buoy. (b) Schematic of second component-chamber. (c) Schematic of outlet and inlet valve – Wafer Swing Check Valve.

where ρ is the fluid density (kg/m^3) (water in this case), $\vec{u}$ is the velocity of fluid (m/s), V_f is the volume fraction, A_f is the area fraction, p pressure (Pa), τ the viscous stress tensor (Pa), G gravity (m/s^2) and F is the fluid fraction. For coupling of the GMO's motion, Eqs. (1) and (2) should be solved in each time step and the situation of all the objects is recorded and the volume fraction is updated by FAVOR technique. Eqs. (5) and (6) can be solved by substitution of $(-\frac{\partial V_f}{\partial t})$ in right-hand side of both equations with the following form:

$$-\frac{\partial V_f}{\partial t} = \overrightarrow{U}_{obj} \cdot \vec{n} S_{obj} / V_{cell} \tag{8}$$

S_{obj}, $\vec{n}\overrightarrow{U}_{obj}$ and V_{cell} are the surface area (m^2), surface normal vector, the velocity of moving object (m/s) in a mesh cell and the total cell volume (m^3) respectively. Eqs. (1) and (2) are solved by the explicit GMO method with the following discretized equations:

Table 1 Different mesh generation.

	Cell number	Mesh block
1	298,320	
2	504,186	
3	723,451	
4	904,450	

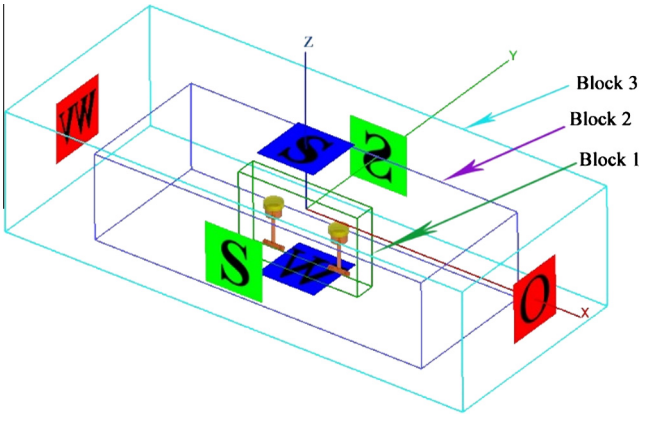

Figure 8 Boundary conditions and mesh blocks.

$$\overrightarrow{F}_h^n + \sum \overrightarrow{F}_i = m\left(\frac{\overrightarrow{V}_G^{n+1} - \overrightarrow{V}_G^n}{\Delta t}\right) \tag{9}$$

$$\overrightarrow{T}_h^n + \sum \overrightarrow{T}_i = [J], \left(\frac{\vec{\omega}^{n+1} = -\vec{\omega}^n}{\Delta t}\right) + \vec{\omega}^n \times ([J], \vec{\omega}^n) \tag{10}$$

The upper indexes are related to time step, and $\sum \overrightarrow{F}_i$ and $\sum \overrightarrow{T}_i$ are the sum of all force and torque elements except hydraulic parts. In each time step, after calculating $\overrightarrow{V}_G^{n+1}$ and $\vec{\omega}^{n+1}$ in the same way, the fluid velocity and pressure field are obtained by duplicately solving the momentum and continuity equations [15].

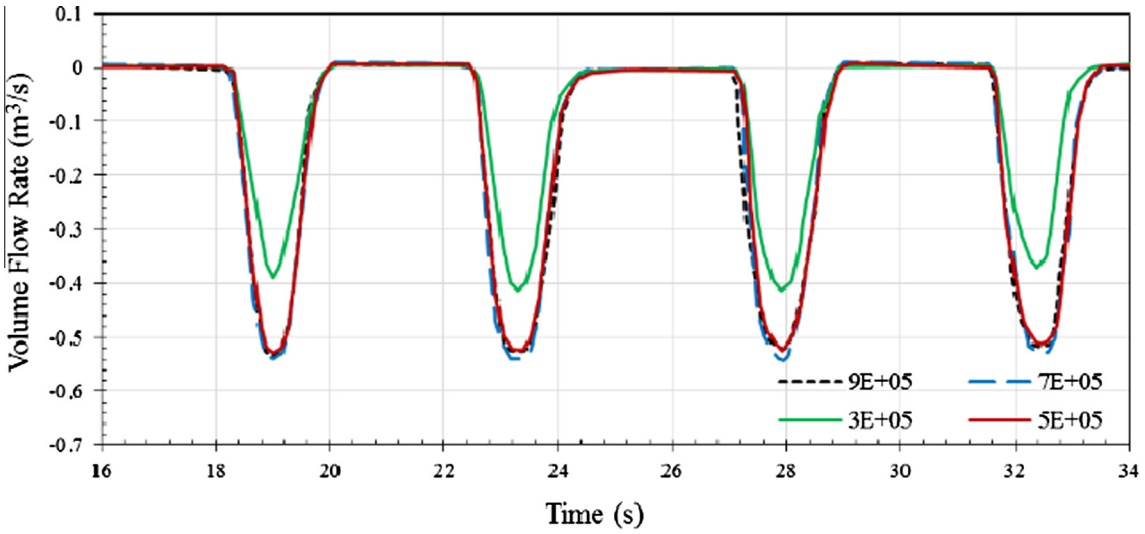

Figure 9 Comparison of outlet volume flow rate for a wave amplitude of 1.25 m.

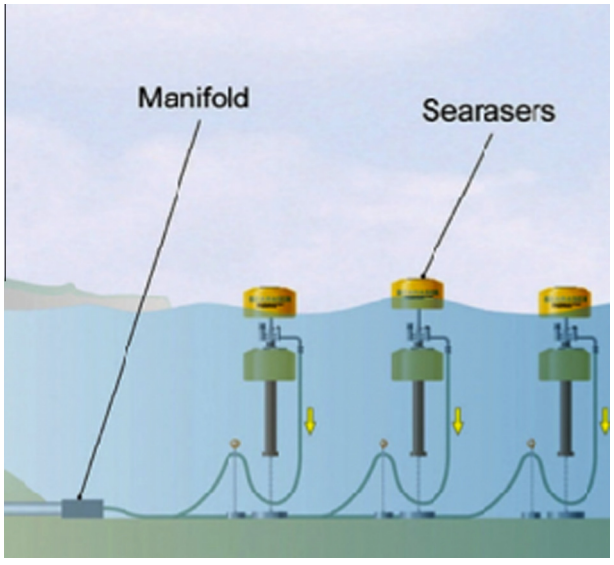

Figure 10 Using multiple Searasers with defined distance in series form.

4. Validation

For evaluating the numerical results in Flow-3D, a point absorber named WRASPA was simulated exactly similar to the experimental model of Bhinder et al. [13], and then the numerical and experimental results were compared. The geometry and dimensions of simulated WRASPA are shown in Fig. 2.

To generate mesh for the wave tank and Searaser, two mesh blocks with varied sizes were applied to improve the accuracy of the results. As shown in Fig. 3a, mesh Block 1 has small grids in which the point absorber was simulated in the middle and mesh Block 2 has larger grids around the Block 1. In Fig. 3b the different boundary conditions of this simulation are shown completely.

In the present investigation, the wave amplitude, time period, and water depth were considered 0.01 m, 1 s and 0.42 m respectively. Also, the mesh number was 963210 whose smallest grid (0.015 m) was generated to model the moving wave inside the tank. In Fig. 3b, the wave tank dimensions of 12.5 m length, 1.5 m width and 0.45 m height are shown. Based on the previous works [16] the RNG $(k-\varepsilon)$ turbulence model was used to solve the turbulent flow because it had acceptable accuracy for this case. The position of buoy (based on the angular movement in radian) for WRASPA was compared in Fig. 4, in which they were in good agreement with each other and their differences can be considered almost negligible except for the vicinity of the peaks.

In Fig. 5 the velocity contours in 1.09 s and 15.75 s are indicated separately. Because the velocity is increased when the wave reaches near the buoy and the angular position is changed while wave is passing the point absorber, the velocity contours are different at the mentioned times. Additionally in Fig. 6, the free surface elevation is shown in 1.09 s and

Table 2 Different wave heights for the south of Caspian Sea [18].

Season	Minimum height (m)	Maximum height (m)
Summer	0.5	1.25
Winter	0.94	2.34

Table 3 Different distances between centers of Searasers.

No.	Distance between two superficial buoys (m)
1	10
2	15
3	20

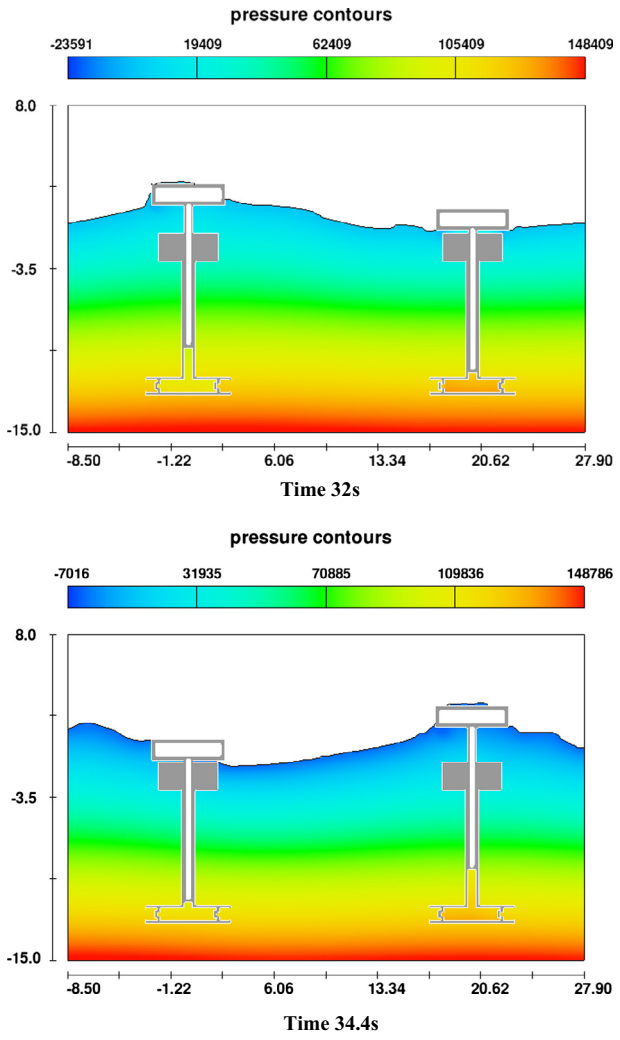

Figure 11 Pressure contour of wave movement in different times 32 s, and 34.4 s.

6.75 s. In fact, this plot demonstrates that the wave shape in the wave tank is varying as time passes.

5. Searaser modeling

5.1. Geometrical dimensions and components

In this study, Alvin Smith's second scheme (modified model) was chosen for simulation including 4 main bodies as follows.

5.1.1. Buoy

The buoy radius and height are 2.6 m and 1.5 m respectively. This buoy is inserted 10.1 m deep in the pumping duct. The radius of this part is considered equal to radius of the pumping case to prevent leakage from the edges. As shown in Fig. 7a, the buoy is not completely filled and a cylindrical space with the radius of 2.3 m and height of 0.5 m is extracted from inside the buoy. As the buoy should overcome the water column of the lower layers and also push the accumulated water, the net weight of this buoy was assigned near 9000 kg. In order to construct this device, specific composite material is usually utilized to prevent the corrosion caused by water, also the buoy should be filled with sand, water and so on to reach the reasonable weight since the composites are lightweight. Furthermore, the buoy was designed to be capable of moving only in vertical direction (the gravity direction) because the vertical duct does not allow it to move toward other directions.

5.1.2. Chamber

According to the Fig. 7b, the inside body for lower buoy is a chamber including inlet and outlet valves with radius of 0.268 m. The radius and height of the upper cylindrical section are 2.1 m and 2 m respectively. In this simulation, the bottom of chamber was assigned to be fixed because it helps the converter to reach the maximum efficiency.

5.1.3. Inlet & outlet valves

In order to select the valve type, three factors should be considered including software limitation to simulate, large diameter of outlet pipe, and valve compatibility to the seawater. According to the research, conducted in this area, Wafer Swing Check Valve can be a suitable choice to assign for this valve, and this kind of valve is indicated in Fig. 7c schematically. According to the valve catalog of the CLA-VAL company

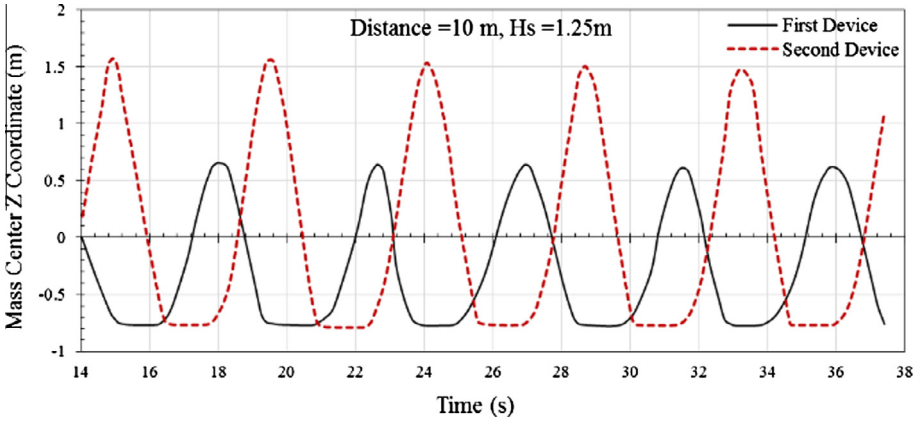

Figure 12 Mass center movement of buoys for wave height of 1.25 m and distance 10 m.

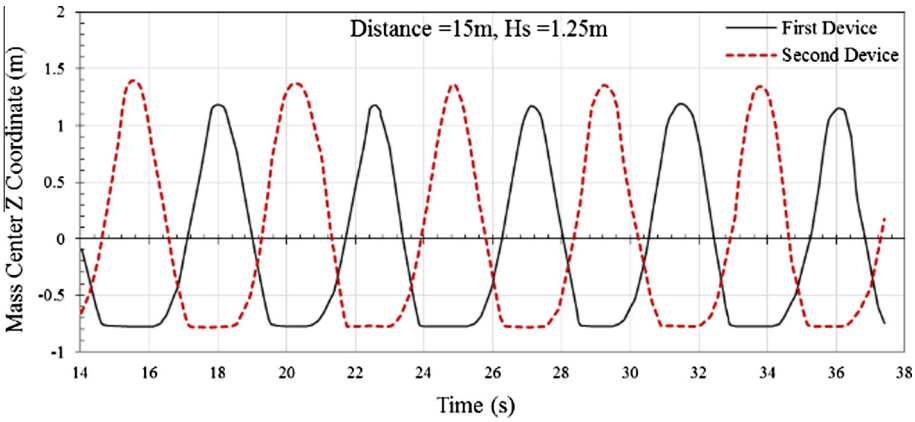

Figure 13 Mass center movement of buoys for wave height of 1.25 m and distance 15 m.

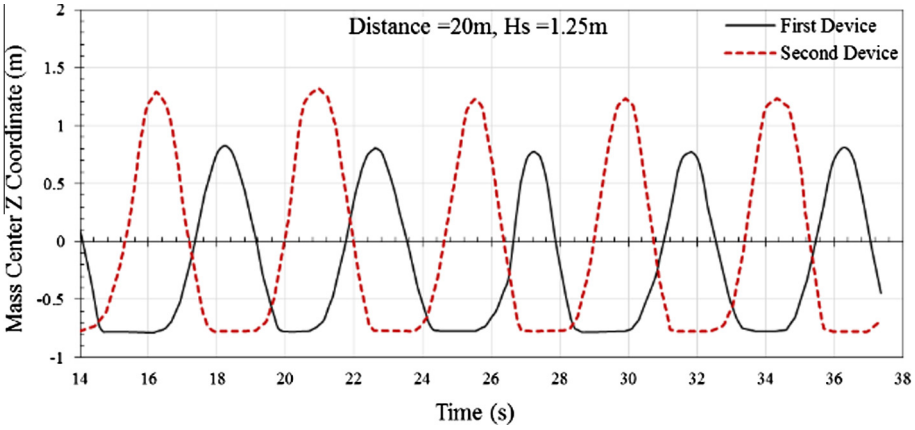

Figure 14 Mass center movement of buoys for wave height of 1.25 m and distance 20 m.

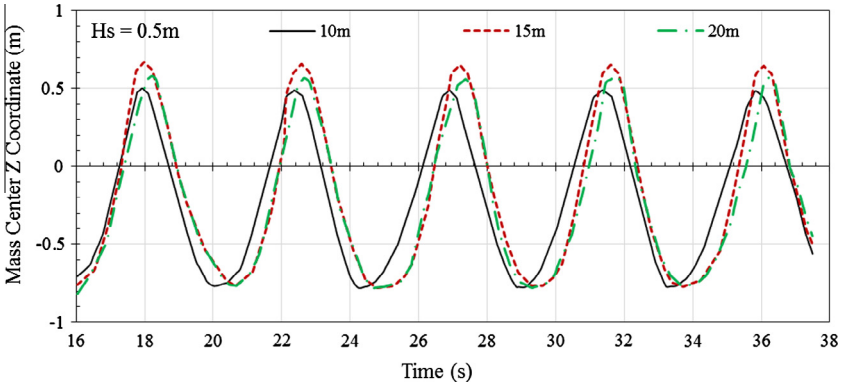

Figure 15 Mass center movement of the first superficial buoy for 0.5 m wave height and distances 10 m, 15 m and 20 m from each other.

[17], this valve was made from Aluminum Bronze ASTM B148, Alloy 95200, so the density was assigned 7.64 g/cm^3 and also the size of B and C sections was designed 0.268 m and 0.4 m respectively. Additionally, the properties of outlet valve were set the same as inlet valve in this modeling.

5.2. Boundary conditions and mesh blocks

In the present work, meshing the solution domain was extremely important because fluid and solid were moving simultaneously. According to the ability of meshing in this software, three mesh blocks were generated with structure type to improve the accuracy of calculations. As indicated in Fig. 8, the X and Y coordinate axes were on the center of upper buoy and Z axis was assigned in direction of ground gravity. In Fig. 8, the abbreviation of WV, S, O, and W stands for wave, symmetry, outflow and wall conditions respectively. In addition, the RNG $(k-\varepsilon)$ turbulence model was utilized to model the turbulent flow while the wave was sinusoidal.

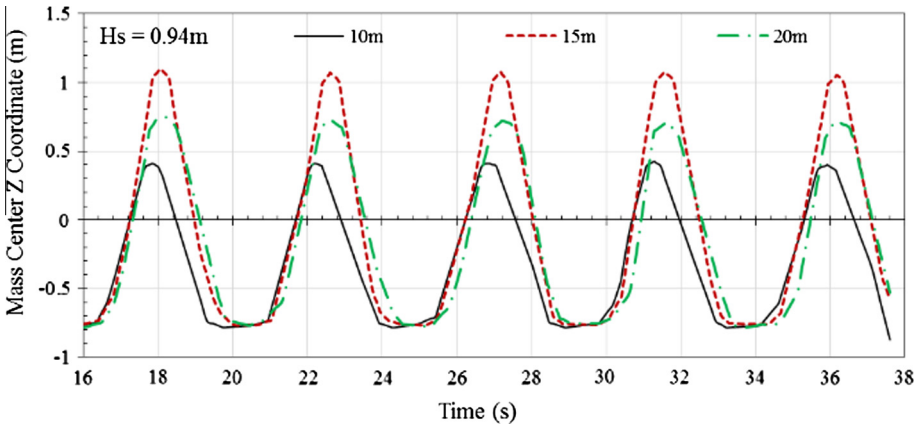

Figure 16 Mass center movement of the first superficial buoy for 0.94 m wave height and distances 10 m, 15 m and 20 m from each other.

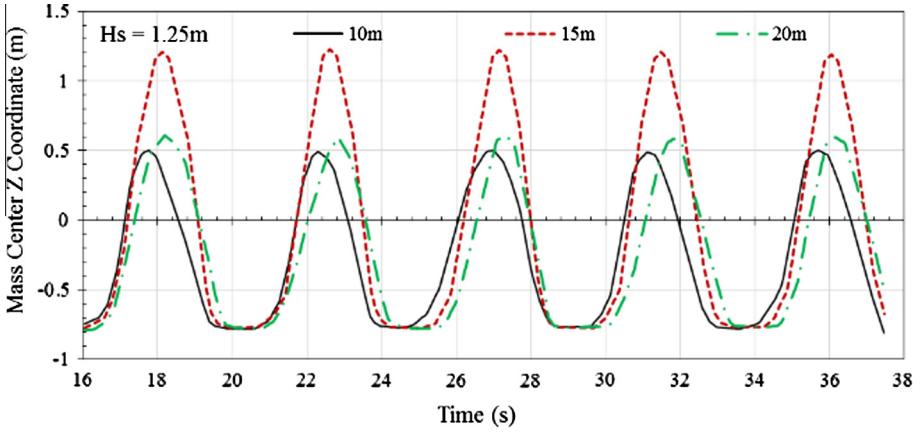

Figure 17 Mass center movement of the first superficial buoy for 1.25 m wave height and distances 10 m, 15 m and 20 m from each other.

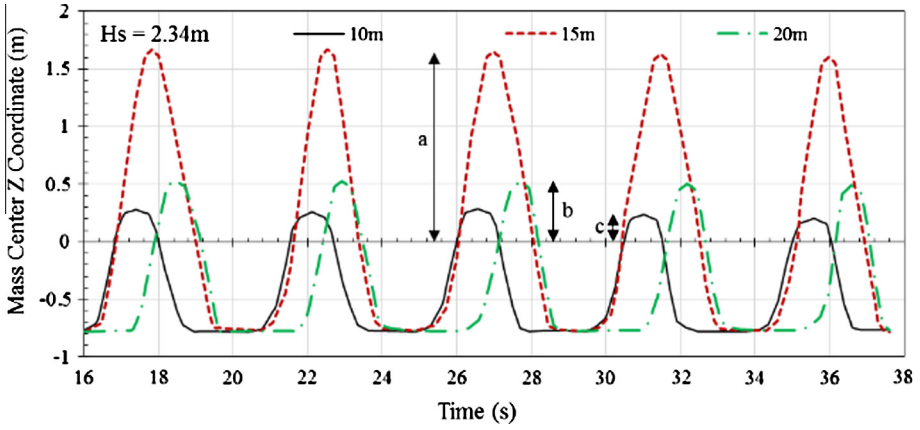

Figure 18 Mass center movement of the first superficial buoy for 2.34 m wave height and distances 10 m, 15 m and 20 m from each other.

6. Grid independency

Grid study is usually essential to obtain the number of a sufficient grid. Therefore in order to accomplish a 3D simulation of Searaser for a moving wave of 1.25 m height, four grids were generated with 298,320, 504,186, 723,451, and 904,450 cell numbers. To enhance the accuracy of the solution, the number of grids in mesh blocks was enhanced as it shown in Table 1. In

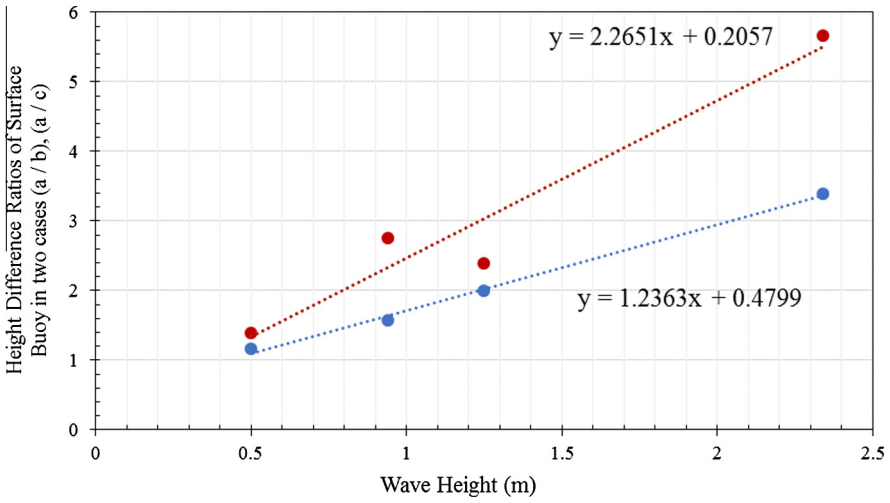

Figure 19 Linear relation between height difference ratio of surface buoy (a/b & a/c) versus various wave heights.

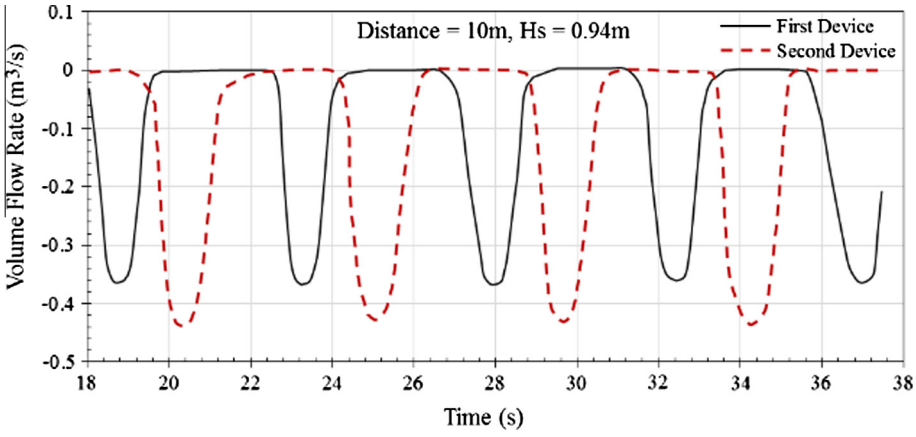

Figure 20 Volume flow rate of buoys with distance 10 m and 0.94 m wave height.

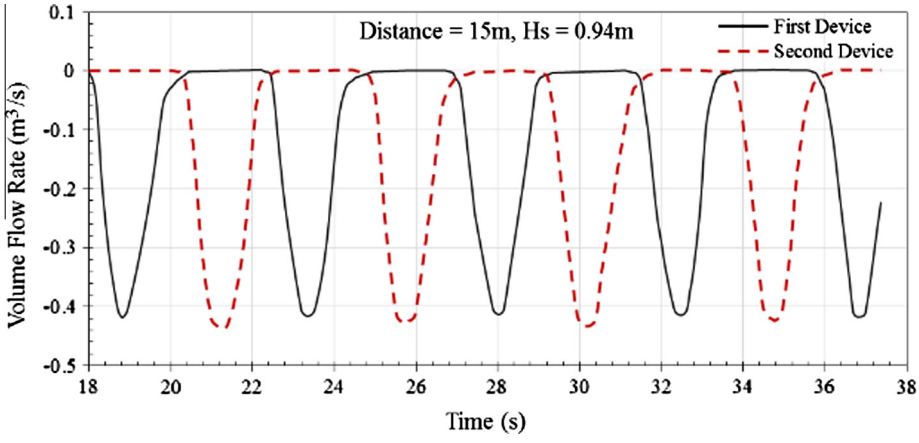

Figure 21 Volume flow rate of buoys with distance 15 m and 0.94 m wave height.

order to choose the best grid among the generated grids, the volume flow rate was measured for various times in the outlet valve and compared together in Fig. 9. As it can be seen in this figure, the grid with 504,186 cells was the best choice for simulation of this investigation.

7. Results and discussion

One way for using the wave energy efficiently is to utilize some Searasers simultaneously. This method is also commonplace

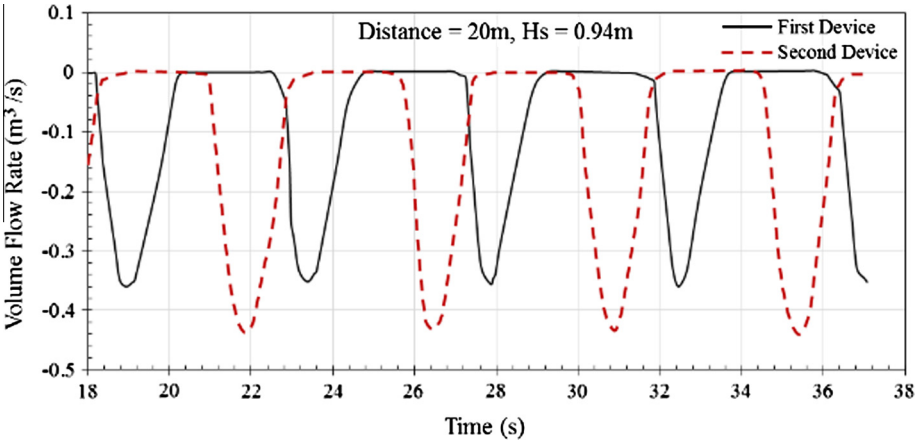

Figure 22 Volume flow rate of buoys with distance 20 m and 0.94 m wave height.

for wind energy. As shown in Fig. 10, in Alvin Smith's invention several buoys were used simultaneously. In this study, two buoys with three different distances were evaluated in four varied wave heights. Additionally, the results of this research can be used for other point absorbers with superficial buoys, because this distance influences on the buoys movements that this movement is the same for other point absorbers.

In this section, the performance of Searaser was evaluated for four wave heights including 0.5 m, 0.94 m, 1.25 m and 2.34 m, because the wave heights for Caspian Sea change based on the Table 2.

In this study, the designed distances for two Searasers are listed in the following table (see Table 3).

In order to have a better understanding, the pressure contour of Searaser in the wave tank is plotted in Fig. 11 for different times including 32 s and 34.4 s. As can be seen in this figure, the wave generation starts from X_{min} moving toward the X_{max} after passing the Searasers. As shown in this figure, the pressure amount increases linearly in the wave tank because the water depth grows up linearly. This phenomenon can be seen in the picture obviously. Fig. 11 shows the buoys response to the wave movements.

In Figs. 12–14 the movement of mass center of the superficial buoys for three different distances 10 m, 15 m and 20 m and for constant wave height of 1.25 m is shown respectively.

As it can be seen in previous figures, the applied force to the second device delays a little while the distance of two Searasers increases. Furthermore, the interaction effects of two buoys lead to some differences in fluctuation domain of superficial buoys. As a result, the superficial buoys of the second Searaser can reach higher altitudes than first buoy. Likewise, Agmalo et al. [19] observed the same results in their studies. To evaluate the performance of the superficial buoys, mass center movement of first buoy in distances 10 m, 15 m and 20 m for four different wave heights was calculated and is shown in Figs. 15–18 respectively.

As it can be seen in the previous figures, approximately the maximum fluctuation is when the buoys are 15 m far from each other. These figures also show that with increasing the wave height, this phenomenon (maximum fluctuation for distance 15 m) intensifies highly. On the other hand, the buoys at distance 15 m show better performance than distances 10 m or 20 m and this benefit demonstrates a linear relationship with increasing wave height (see Fig. 19). To clarify this phenomenon, the ratios of a/b and a/c (defined in Fig. 18) were depicted separately versus different wave heights in Fig. 19. As it can be seen in this figure, when wave height increases, the ratio of a/b and a/c goes up linearly. Therefore, when mass center of buoy for distance 15 m raises more than two other distances, its performance will be much better on account of this increment.

The volume flow rate of outlet valve for three different distances of buoys (10 m, 15 m, 20 m) and constant wave height of 0.94 m is shown in Figs. 20–22 respectively.

A common reason for using multiple devices is to have stable outlet flow rate. Stabilizing the outlet flow rate causes to produce uniform electricity and reduce fluctuation in electricity production and it is of high importance when the electricity is produced and used at the same time. The best way of stabilizing the outlet flow rate is to synchronize the maximum volume flow rate (VFR) of one device with the minimum VFM of another device. As shown in Figs. 20–22, the difference between maximum outlet VFR for first device (Black Line) and maximum outlet VFR for second device (red Line) increases gradually when the distance between two devices raises. As it is obvious in these figures, the maximum VFR of first device is synchronized with the minimum VFR of another device when the devices are 15 m far from each other. In all three distances of devices, the amount of pumping water that is produced by the second device is more than the first one and it is compatible with results of Agmalo et al. [19]. In addition, the results show that for all three distances of buoys, the second device pumps more water than the first one. When the devices are in 15 m distance from each other, the difference of outlet flow rate for two devices is negligible in comparison with distances 10 and 20 m. This feature causes to have more stable flowrate that is compatible with the results of Agmalo et al. [19].

8. Conclusion

In the recent years, ocean wave energy converters have been evaluated to find the most appropriate systems to harvest the wave energy in Caspian Sea. Hence, the commercial software (Flow-3D) was utilized to simulate a novel wave energy con-

verter named Searaser by an inventor named Alvin Smith. In this simulation, the upper buoy of the converter was assigned to move up via the ocean waves generated in a 3D numerical wave tank. In this work for validating the outcomes, a wave buoy was modeled and its results were compared with the experimental results and showed good agreements. In this article the effect of buoy distance in hydrodynamic performance of Searasers was studied precisely. Three distances of 10, 15 and 20 m were considered. The outlet flow rate curves and buoy movement curves were depictured. The results showed that the optimum distance of buoys between these three distances is 15 m due to the following reasons:

1- Both of the buoys can go up higher altitude in the pumping chamber and the outlet flow rate maximize in this distance.
2- In the outlet volume flow rate curve, the maximum outlet VFR of one device is synchronized with the minimum outlet VFR of the other device. Hence, this phenomenon can stabilize the outlet flow rate and decrease the fluctuation of electricity generation.
3- For all the wave heights, the difference in outlet flow rate of the devices is insignificant so the water pumping is more stable and the electricity generation shows less fluctuation.

References

[1] A. Muetze, J.G. Vining, Ocean wave energy conversion – a survey, in: Industry Applications Conference, 2006, 41st IAS Annual Meeting, Conference Record of the 2006 IEEE.3, 2006, pp. 1410–1417.

[2] J.P. Kofoed, P. Frigaard, E. Friis-Madsen, H.C. Sørensen, Prototype testing of the wave energy converter wave dragon, Renew. Energy 31 (2006) 181–189.

[3] D. Vicinanza, P. Frigaard, Wave pressure acting on a seawave slot-cone generator, Coast. Eng. 55 (6) (2008) 553–568.

[4] D. Vicinanza, F. Ciardulli, M. Buccino, M. Calabrese, J.P. Kofoed, Wave loadings acting on an innovative breakwaters for energy production, in: The International Coastal Symposium, 2011, pp. 608–612.

[5] D. Vicinanza, L. Margheritini, J.P. Kofoed, M. Buccino, The SSG wave energy converter: performance, status and recent developments, Energies 5 (2) (2012) 193–226.

[6] H. Fernandez, G. Iglesias, R. Carballo, A. Castro, J.A. Fraguela, F. Taveira-Pinto, M. Sanchez, The new wave energy converter wavecat: concept and laboratory tests, Marine Struct. 29 (1) (2012) 58–70.

[7] G.J. Dalton, R. Alcorn, T. Lewis, Case study feasibility analysis of the pelamis wave energy converter in Ireland, Portugal and North America, Renew. Energy 35 (2) (2010) 443–455.

[8] R. Henderson, Design, simulation, and testing of a novel hydraulic power take-off system for the pelamis wave energy converter, Renew. Energy 31 (2) (2006) 271–283.

[9] F.D.O. Antonio, Wave energy utilization: a review of the technologies, Renew. Sustain. Energy Rev. 14 (3) (2010) 899–918.

[10] R. Alamian, R. Shafaghat, S.J. Miri, N. Yazdanshenas, M. Shakeri, Evaluation of technologies for harvesting wave energy in Caspian Sea, Renew. Sustain. Energy Rev. 32 (2014) 468–476.

[11] V. Heller, J.R. Chaplin, F.J.M. Farley, M.R. Hann, G.E. Hearn, Physical model tests of the anaconda wave energy converter, in: Proc. 1st IAHR European Congress, 2000.

[12] J. Pastor, Y. Liu, Hydrokinetic energy: overview and it's renewable energy potential for the Gulf of Mexico, in: Green Technologies Conference, IEEE, 2012, pp. 1–3.

[13] M. Bhinder, C. Mingham, D. Causon, M. Rahmati, G. Aggidis, R. Chaplin, Numerical and experimental study of a surging point absorber wave energy converter, in: Proceedings of the 8th European Wave and Tidal Energy Conference, 2009.

[14] A. Smith, PUMPING DEVICE, Patent Application Publication, US 2013/0052042 A1, February 28, 2013.

[15] C.W. Hirt, B. Nichols, Flow-3D User's Manual, Flow Science Inc., 1988.

[16] B.H. Choi, D.C. Kim, E. Pelinovsky, S.B. Woo, Three-dimensional simulation of tsunami run-up around conical Island, Coast. Eng. 54 (8) (2007) 618–629.

[17] Cla-Val company, Wafer Swing Check Valve, <www.cla-val.com>.

[18] E. Rusu, F. Onea, Evaluation of the wind and wave energy along the Caspian Sea, Energy 50 (2013) 1–14.

[19] E.B. Agamloh, A.K. Wallace, A. Von Jouanne, Application of fluid–structure interaction simulation of an ocean wave energy extraction device, Renew. Energy 33 (4) (2008) 748–757.